Palaeogeography, Palaeoclimatology, Palaeoecology 654 (2024) 112440

Contents lists available at ScienceDirect

Palaeogeography, Palaeoclimatology, Palaeoecology

journal homepage: www.elsevier.com/locate/palaeo

Organic carbon isotope ($\delta^{13}C_{org}$) curve and extinction trends across the Triassic/Jurassic boundary at Mt. Sparagio (Italy): A tool for global correlations between peritidal and pelagic successions

Manuel Rigo [a,b,*], Marco Favero [a], Pietro Di Stefano [c], Simona Todaro [c]

[a] Department of Geosciences, University of Padova, Padova 35131, Italy
[b] IGG-CNR, Padova 35131, Italy
[c] Department of Earth and Marine Sciences, University of Palermo, Palermo 90123, Italy

ARTICLE INFO

Editor: A Ferretti

Keywords:
Triassic
Jurassic
Mass extinction
Carbonate platform
Pelagic
Carbon isotopes
Organic matter

ABSTRACT

The Triassic/Jurassic boundary (TJB, 201.3 Ma) is characterized by profound turnovers in both marine and terrestrial biota, known as end-Triassic mass Extinction event (ETE). During this severe event, distinct negative carbon isotope excursions (CIEs) have been globally observed, and they were linked to volcanogenic emissions or methane release by dissociation of clathrates. The triggering factor of the negative CIEs was attributed to the emplacement of the Central Atlantic Magmatic Province (CAMP) and the break-up of the Pangea. Specifically, three significant carbon-cycle disruptions named Precursor, Initial and Main CIE have been recorded in several stratigraphic successions deposited in terrestrial and pelagic environments. We investigated the organic carbon isotope curve from the subtidal facies of the Mount Sparagio section (Sicily, Italy), which is a continuous peritidal succession representing an Upper Triassic to Lower Jurassic carbonate platform edging the south-western side of the Tethys Ocean. For the first time, we achieved a complete profile of organic carbon stable isotopic composition ($\delta^{13}C_{org}$) during the end-Triassic mass Extinction event (ETE) in a carbonate shallow water environment. The $\delta^{13}C_{org}$ profile highlights the 3 negative excursions that characterized the Triassic/Jurassic boundary time interval in pelagic and deep-water successions. The documented CIEs correspond to significant biotic turnovers recognized along the Mt. Sparagio section, suggesting that also the Upper Triassic-Lower Jurassic carbonate platforms were affected by the onset of the Central Atlantic Magmatic Province. Furthermore, although the Mt. Sparagio section has been studied in detail for microfacies associations and it is well biostratigraphically constrained with shallow marine macro- and microfossils, only the documented $\delta^{13}C_{org}$ negative shifts allowed to correlate peritidal environments to pelagic successions, making the organic carbon curve ($\delta^{13}C_{org}$) a powerful tool for global correlations.

1. Introduction

The Triassic-Jurassic boundary (TJB) is a time interval of profound faunal and floral turnover, characterized by a severe biotic crisis recorded in both terrestrial and marine system (Hesselbo et al., 2002; Kiessling et al., 2007; Ruhl et al., 2010; Todaro et al., 2017, 2023; Zaffani et al., 2018; Du et al., 2020, 2023). This event is one of the Big Five mass extinctions occurred in the Phanerozoic and it is known as end-Triassic mass Extinction event (ETE) (Raup and Sepkoski Jr, 1984). The trigger episode suggested for the ETE is the emplacement of the Central Atlantic Magmatic Province (CAMP) along with the beak-up of the supercontinent Pangea (Hesselbo et al., 2002; Marzoli et al., 1999, 2004; Nomade et al., 2007; Zaffani et al., 2018) that might have led significant climate and environmental alterations by the emission of important amount of volcanogenic CO_2 and release of biogenic methane starting in the latest Rhaetian (Davies et al., 2017; Ruhl et al., 2011). As consequence of the greenhouse gas discharge, a prolonged global warming (McElwain et al., 1999) followed by a sudden cooling event (Todaro et al., 2023) occurred across the TJB, with a stratification of the sea water and change of the oceanic circulation (Huynh and Poulsen, 2005), inducing the spreading of dysoxic conditions and decreasing of the biological pump efficiency (Greene et al., 2012; Hallam and Wignall, 1999; He et al., 2020, 2022; Pálfy et al., 2001). The CO_2 emission into the atmosphere by the CAMP has also influenced the carbon cycle (Ruhl

* Corresponding author at: Department of Geosciences, University of Padova, Padova 35131, Italy.
E-mail address: manuel.rigo@unipd.it (M. Rigo).

https://doi.org/10.1016/j.palaeo.2024.112440
Received 23 February 2024; Received in revised form 4 July 2024; Accepted 4 August 2024
Available online 17 August 2024

et al., 2011; Schaller et al., 2012; Zaffani et al., 2018) with direct consequence on the carbonate productivity (Greene et al., 2012; Van De Schootbrugge et al., 2008), especially in shallow water environments (Todaro et al., 2017, 2018, 2023). In fact, the increase of CO_2 in hydrosphere might have intensified the dissolution of CO_2, resulting in ocean acidification that affected the biomineralization of the organisms with a carbonate shells, such as sponges, corals, bivalves and foraminifers (Črne et al., 2011; Flügel, 2002; Kiessling et al., 2007; Todaro et al., 2017, 2023). Furthermore, the increase of biogenic methane and CAMP volcanogenic carbon release have been recorded globally on the organic carbon isotope system, resulting in 3 negative carbon isotope excursions (CIEs) that have been named in stratigraphic order as Precursor, Initial and Main CIEs. The first 2 CIEs are uppermost Rhaetian in age, while the Main CIE ranges across the TJB (Pálfy et al., 2001, 2007; Ward et al., 2001, 2004, 2007; Hesselbo et al., 2002; Guex et al., 2004; Ruhl et al., 2009; Kuroda et al., 2010; Ruhl and Kürschner, 2011; Hillebrandt et al., 2013; Thibodeau et al., 2016; Yager et al., 2017, 2021; Fujisaki et al., 2018; Zaffani et al., 2018; Du et al., 2020, 2023). Nevertheless, these 3 negative CIEs refers to the bulk organic matter in the rock sample, which consists of different compounds that have specific values of $\delta^{13}C_{org}$. These components might contribute relatively to the $\delta^{13}C_{org}$ archives, without necessarily requiring possible perturbations in the isotopic composition of the ocean and atmosphere systems (Van De Schootbrugge et al., 2008; Bartolini et al., 2012; Zaffani et al., 2018; Rigo et al., 2020). However, similar isotopic trends have been found in coeval sections at different locations and depositional environments across the TJB, suggesting a worldwide shared history and trigger factor, regardless of their specific values (Bartolini et al., 2012; Zaffani et al., 2018), as also documented for other Triassic time interval close to the TJB such as the Norian/Rhaetian boundary (Rigo et al., 2020, 2024).

Although the ETE has been deeply investigated, a direct correlation of the biotic turnovers and physical events (e.g. expansion of dysoxic conditions) between pelagic basins and carbonate platforms is still missing due to the different index fossils used as biostratigraphic markers and the absence of other physical stratigraphic tools useful for correlation (e.g. magneto- and cyclostratigraphy, radiometric ages). We thus studied the organic carbon isotopic composition of Mt. Sparagio section (Sicily, Italy) (Todaro et al., 2017, 2018, 2022b, 2023; He et al., 2020, 2022), that represents a continuous peritidal succession edging the south-western side of the Tethys Ocean across the TJB, in an effort to describe a common physical tool for global correlations.

2. Geological setting

The studied section is located in the San Vito Lo Capo Peninsula in north-western Sicily (Fig. 1). This area belongs to the Apennine-Maghrebian fold and thrust belt and consists of a pile of south-verging thrust sheets that were accreted during Miocene and early Pliocene times (Abate et al., 1991; Giunta and Liguori, 1972). Successively, the thrust system has been dissected by Pliocene and Pleistocene normal and strike-slip faults mostly related to the Tyrrhenian extension (Nigro and Renda, 2002) (Fig. 1 A, B). The stratigraphic architecture of the thrust sheets in this area consists of Upper Triassic to Miocene carbonate successions. In particular, in the southern area of the San Vito Lo Capo Peninsula, the Mt. Sparagio thrust crops out as a W-E oriented elongated ridge of about 15 Km. This ridge consists of Mesozoic marine successions, up to 1500 m in thickness, and it is represented in stratigraphic order by Upper Triassic-lowermost Jurassic peritidal cycles draped by Middle-Upper Jurassic Ammonitico Rosso limestone, which is covered by Cretaceous rudist breccias interpreted as slope debris and talus aprons (Randazzo et al., 2020, 2021). Lower Miocene glauconitic calcarenites follow upward through a deep erosional truncation.

The studied section crops out along the northern slope of the Mt. Sparagio ridge, close to the village of Custonaci, in a locality known as the Mt. Cocuccio (38°05′N, 12°51′E) (Fig. 1 C, D). The section consists of an about 400 m thick monotonous succession of peritidal cycles straddling the Triassic/Jurassic boundary. Paleogeographically, it belonged to a large Mesozoic carbonate platform that edged the western termination of the Tethys (Siculo-Tunisian platform sensu Di Stefano et al., 1996; Todaro et al., 2022a).

The cycles show an average thickness of about 1.5 m, and they regularly consist by three shallowing-upward lithofacies, with a subtidal facies prograding on an erosional surface, overlain by an intertidal stromatolitic facies and, in turn, by a reddish, yellowish or greenish paleosoil. On the base of the macro and micropaleontological associations in the subtidal facies three units have been differentiated from the base: 1) Unit A, about 111 m thick, contains a very diversified association of large megalodontoids (*Megalodon* spp. and *Dicerocardium* spp.)

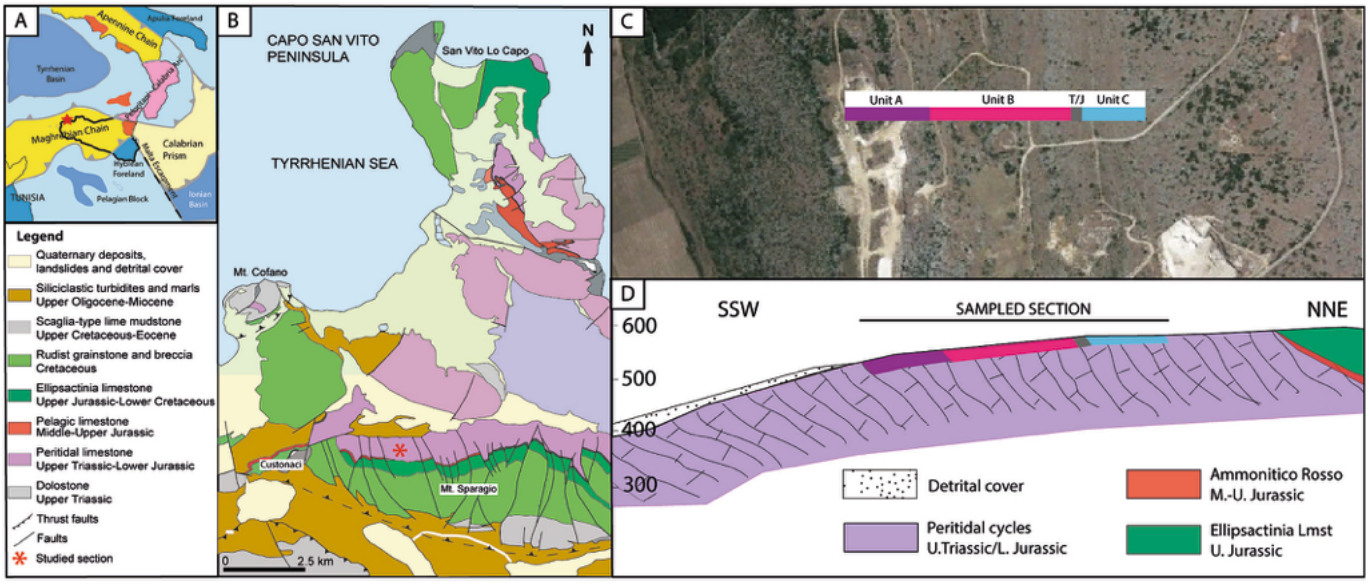

Fig. 1. A) Location of the studied section (red star) in a simplified tectonic sketch of the Central Mediterranean area; B) Geology of the Capo San Vito Peninsula (mod. after Abate et al., 1991): the red asterisk indicates the sampled section along the northern slope of Mt. Sparagio. C) Google Earth image (plain view) of the studied locality and D) geological cross section of the sampled section. (For interpretation of the references to colour in this figure legend, the reader is referred to the web version of this article.)

and benthic foraminifers among which *Triasina hantkeni*; 2) Unit B, about 179 m thick, shows a drastic decrease of the biodiversity and size of the megalodontoids still associated to *Triasina hantkeni*; 3) Unit C (140 m thick) records the disappearance of megalodontoids and Triassic benthic foraminifers and the presence of the opportunistic incertae sedis *Thaumatoporella parvovesiculifera* and *Aeolisaccus* sp. Between Unit B and C, a barren interval of about 10 m is assumed as the Triassic/Jurassic boundary (Todaro et al., 2018, 2023).

The high biodiversity of the bivalve community recorded in the Unit A suggests a climatic optimum during the latest Rhaetian, with temperatures up to 30 °C (Todaro et al., 2023), reflecting the maximum SST (sea surface temperature) that a tropical shallow water carbonate platform (T-factory) can tolerate (Laugié et al., 2019). The drastic reduction of the bivalve biodiversity between Unit A and Unit B was interpreted as a precursor of the End Triassic Extinction and coincides to a quick cooling phase (down to 18 °C) as suggested by high $\delta^{18}O_{carb}$ values (Todaro et al., 2023). A second dramatic event corresponding to the extinction of the Rhaetian bivalve community is recorded at the TJB (between Unit B and C), with a remarkable decrease in temperature of >30°, during which the peritidal water temperature cooled down to few degrees (5 °C) (Todaro et al., 2023). These two extinction pulses recorded in the bivalve community well also correlate to the two negative $\delta^{13}C_{carb}$ excursions Initial-CIE and Main-CIE (Todaro et al., 2018, 2022a, 2022b, 2023). The extinction of Rhaetian bivalves and Rhaetian biotic association is also related to an expansion of oceanic anoxia, as recorded by the positive shift of the $\delta^{34}S_{CAS}$ combined with I/(Ca + Mg) record from the top of Unit B of the Mt. Sparagio section that provide evidence of oxygen decline in the western Tethys peritidal environments during the ETE (He et al., 2020, 2022). Moreover, the Zn, Pb, Sr isotopic signatures documented in the Mt. Sparagio section confirmed the impact of CAMP to the ETE. In particular, Zn isotopic values in the median-upper part of Unit B and in the barren interval proved a typical riverine input of magmatic rocks and the unusually low radiogenic $^{87}Sr/^{86}Sr$ signature combined with Pb isotopes match the compositional field of CAMP volcanism either in the form of eroded particulate materials or volcanic fallout (Todaro et al., 2022a, 2022b).

3. Material and methods

Carbonate carbon ($\delta^{13}C_{carb}$) was previously investigated and interpreted by Todaro et al. (2018, 2023). We thus focused on organic carbon ($\delta^{13}C_{org}$) for better correlations between TJB sections deposited in widely separated sedimentary environments (e.g. shallow marine versus deep water environments) and to understand if the three emissions of volcanogenic gas by the CAMP suggested as main trigger events for the ETE (e.g Davies et al., 2017; Zaffani et al., 2018; Du et al., 2020) might have affected also the peritidal carbonate platforms. We thus analyzed 106 samples previously selected from the subtidal facies of the Mount Sparagio section, starting from 92 m the base of Unit A, avoiding possible modern organic matter contamination. The lower part of Unit A (from 0 to 91 m) was not sampled because this part of the section crops out in an active quarry. However, samples and images for biostratigraphic purposes from this part of Unit A were collected during 2015, when the quarry was still inactive (see Todaro et al., 2017).

All the samples were washed with millipore water (15 g), dried in oven at 40 °C overnight, and then reduced into subcentimetric fragments. The fragments were then attacked by a solution of 10% HCl overnight (at least 12 h). Successively, the solution was neutralized in millipore water and the residues were dried at 40 °C overnight and eventually wrapped in tin capsules for $\delta^{13}C_{org}$ analyses. The samples were analyzed at the Department of Geosciences of the University of Padova by using a Delta V Advantage mass spectrometer connected to a Flash HT Elemental Analyzer via the ConFlo IV interface, along with isotope international and in-house standards and multiple blank capsules. Before the calibration against IAEA CH-6 (= −10.45‰) and IAEA CH-7 (= −32.15‰) (Coplen et al., 2006) following the two-point calibration method, the raw data were corrected for the blank contribution. The standard deviation of the in-house standard (ZER = −26.00‰) was better than 0.2‰ during the period of analyses.

To identify any diagenetic alteration that might have affected the carbon isotope primary signal, the samples were previously studied as thin sections (Todaro et al., 2017, 2018) and also scanned with SEM (FESEM-JEOL) to exclude the presence of dolomite by measuring the wt % of Mg2+ (0.2–0.7) at the Department of Chemical Engineering of University of Palermo (Italy) (Todaro et al., 2018, 2022a, 2022b). Other observations to confirm the negligible influence of diagenetic processes were carried out with cathodoluminescence and elemental indicators, such as Mg/Ca, Mn/Sr (He et al., 2020, 2022).

Furthermore, we randomly tested several samples after the acid attack to prove the absence of carbonates (e.g. calcite, dolomites) in the residues before running the $\delta^{13}C_{org}$ isotope analyses. We thus performed X-ray powder diffraction (XRPD) analyses by using a Philips X'Pert Pro MPD diffractometer. This instrument works with a Co anode source, long fine focus, set to 40 kV – 40 mA and the θ/θ geometry is based on a 240 mm radius vertical goniometer. Incident beam setup includes the Bragg-Brentano^{HD} (BBHD) module, divergence slits of ¼°, antiscatter slits of 1° and Soller slits of 0.04 rad. The diffracted beam path is composed of antiscatter slit of 9.1 mm aperture, Soller slits of 0.04 rad and X'Celerator Position Sensitive Detector with a 2.122° 2θ active length. Measurements were carried out between 3° and 85° 2θ angle, using a 0.017° step size, counting 100 s per virtual step on a spinning sample (1 revolution per second). Samples were prepared using the front-loading procedure over a zero-background Si-crystal sample holder, manufactured to give no diffraction lines. Total scan time is 1 h and 6 min for each sample. Minerals were identified using High Score (Plus) version 4.9.0 by PANalytical B.V., Almelo, The Netherlands (Degen et al., 2014), by means of ICSD (2016–1), PDF-2 (2002) and COD (2021) databases.

4. Results

After acid digestion, all the studied samples bear principally phylloslicates and clay minerals, with k-feldspar and titanium dioxide as minor components, without any piece of evidence of crystalline carbonates. The powder diffraction files are reported for each sample on the online materials.

The resulting $\delta^{13}C_{org}$ profile shows a negative trend starting from the base of the studied segment from −22.8‰ to −26.6‰, followed by a positive trend reaching the value of −21.6‰. This negative-positive trend developed from the uppermost part of Unit A up to the basal most part of Unit B (Fig. 2). A quick negative shift up to the minimum value of −27.6‰ follows, which rapidly returns to the maximum value of −21.3‰.

A second back and forth peak apparently occurred in the lower part of Unit B, before the beginning of a prolonged negative trend (Fig. 2).

After these 2 prominent and significant shifts, a long trend to more negative value is recorded up to the end of Unit B, followed by a stable period along Unit C, where the profile is characterized by minor oscillations with a mean value around −26.2‰ (Fig. 2). It is noteworthy that a clear positive shift of ca. 4‰ is evident between Unit B and C, above the suggested biostratigraphic Triassic/Jurassic boundary (Fig. 2). We prudentially prefer to not connect the two values of −22.1‰ at m 190.1 and 24.2‰ at m 245.6 to the Mt. Sparagio $\delta^{13}C_{org}$ curve, because they do not apparently align with the general trend of the carbon organic profile, and they have been here interpreted as outliers (Fig. 2).

5. Discussion

5.1. Correlation of $\delta^{13}C_{org}$ fluctuations at Mt Sparagio

The $\delta^{13}C_{org}$ values from Mt. Sparagio permit the construction of a complete C organic profile from upper Rhaetian to lower Hettangian,

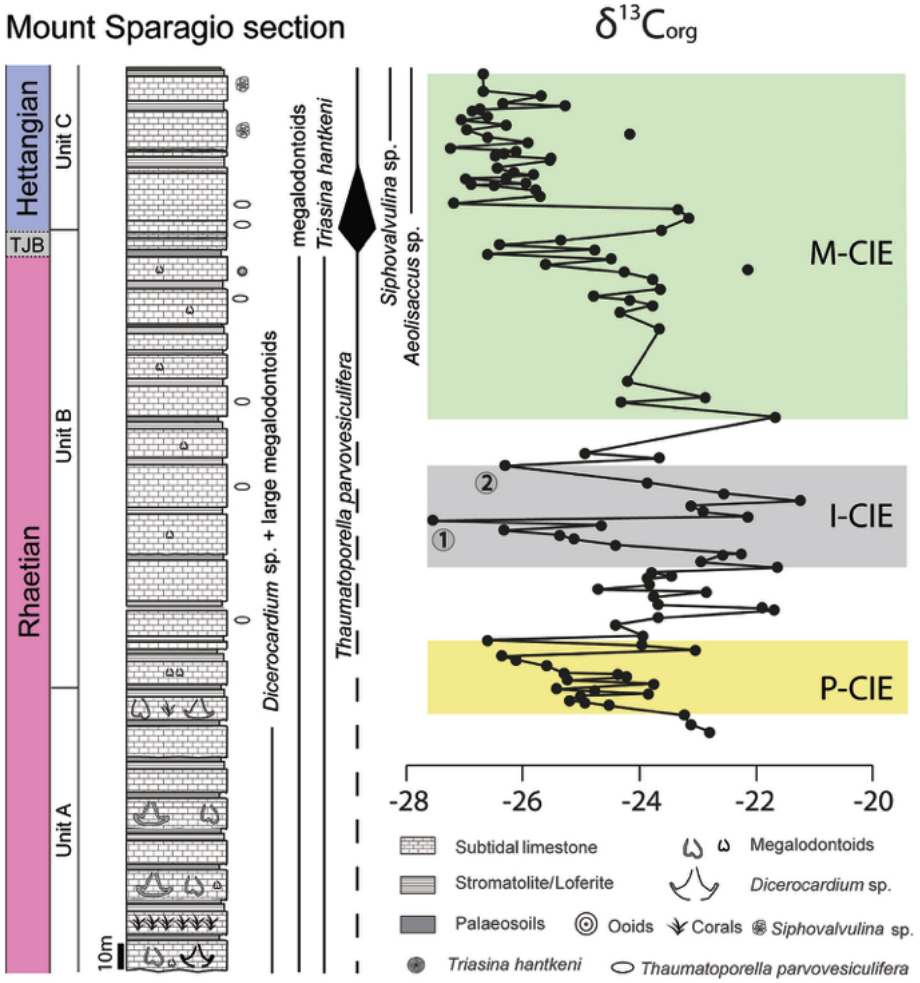

Fig. 2. Stratigraphic log of Mt. Sparagio section with lithostratigraphy and the extension of the lithofacies Unit A, B, and C firstly described by Todaro et al. (2017). Biostratigraphy and the main bioevents are illustrated along the stratigraphic log. The $\delta^{13}C_{org}$ profile is reported with the identification of the 3 main negative carbon excursions characterizing the TJB time interval that are in stratigraphic order the Precursor (P-CIE), Initial (I-CIE) characterized by 2 peaks, and Main CIE (M-CIE).

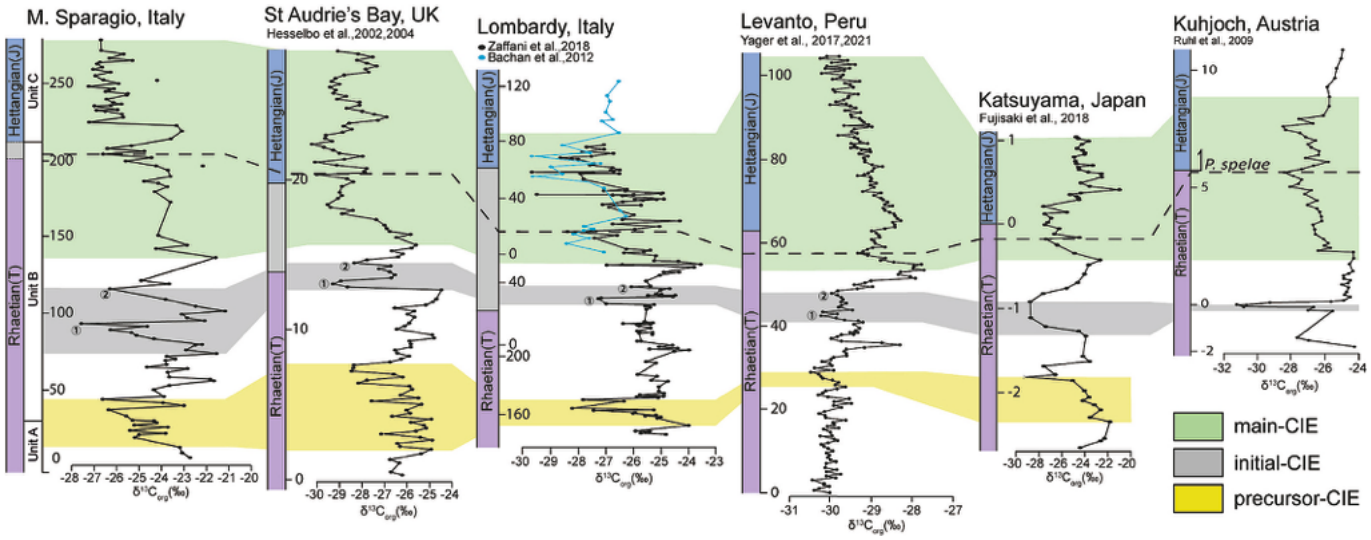

Fig. 3. Chemostratigraphic correlation by using the $\delta^{13}C_{org}$ curves among selected TJB sections in which the 3 CIEs have been clearly documented. Noteworthy is the double peak of the I-CIE in those sections with a detailed $\delta^{13}C_{org}$ profiles. The yellow, gray, and green horizontal bars represent the negative P-CIE, I- CIE and M-CIE respectively. The dashed line marks the Triassic/Jurassic boundary defined in Kuhjoch section (Austria), GSSP of the Hettangian stage, by FO of ammonite *Psiloceras spelae* (Hillebrandt et al., 2013). (For interpretation of the references to colour in this figure legend, the reader is referred to the web version of this article.)

recorded for the first time in a continuous peritidal succession of a carbonate platform in the Tethys Ocean (Fig. 2). Across the Triassic/Jurassic boundary (TJB) of the Mt. Sparagio succession we recognized three prominent perturbations of the $\delta^{13}C_{org}$ that have been interpreted, in stratigraphic order, as precursor (P-CIE), initial (I-CIE) and main (M-CIE) carbon isotope excursion (Figs. 2, 3). These CIEs are consistent with those recognized in other TJB sections, deposited at different latitudes and side of the Pangea, and they have been recorded worldwide in both carbonate and organic carbon systems and in different sedimentary environments such as a mixed terrigenous-carbonate ramp, pelagic open marine basins, and even below the CCD (e.g. Pálfy et al., 2001, 2007; Ward et al., 2001, 2004, 2007; Hesselbo et al., 2002; Guex et al., 2004, Guex et al., 2012; Ruhl et al., 2009; Kuroda et al., 2010; Ruhl and Kürschner, 2011; Thibodeau et al., 2016; Yager et al., 2017, 2021; Zaffani et al., 2018; Fujisaki et al., 2018; Du et al., 2020, 2023)(Fig. 3). The record of almost simultaneous perturbations in both carbonate and organic carbon systems (Precursor, Initial, Main CIEs) indicates an external source of CO_2 (volcanic gas by CAMP) that affected the climatic and environmental stability across the TJB, inducing the ETE.

Across the uppermost part of Unit A (=base of the studied segment) and the lowermost part of Unit B, we documented the P-CIE characterized by a negative excursion of ca. 4‰ (Figs. 2, 3). It is noteworthy that

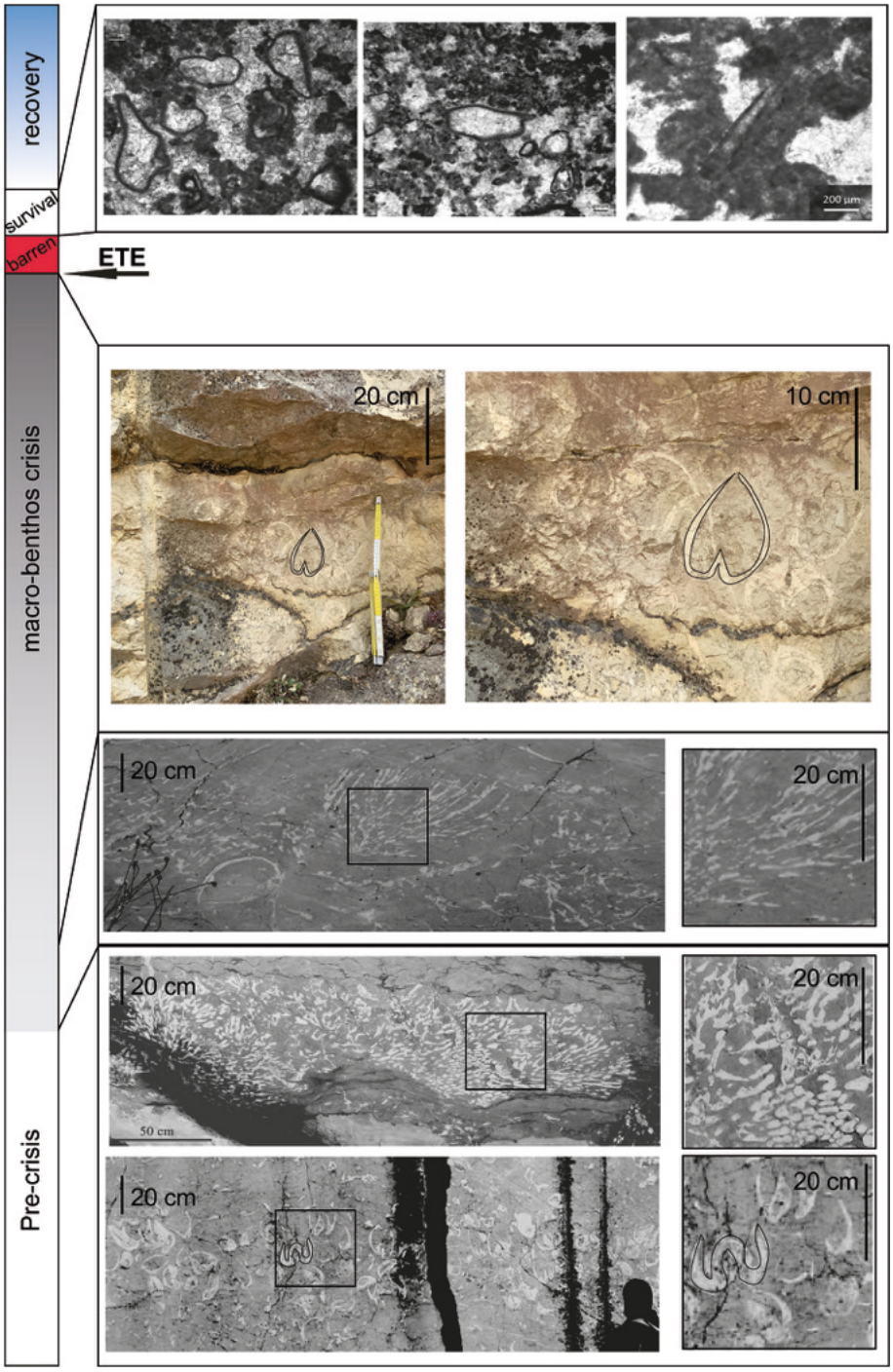

Fig. 4. Biostratigraphy and the main bioevents illustrated along the Mt. Sparagio section. Outcrop photos and details show the macrobenthos communities before, at the beginning and during the calcification crisis. Survival interval is characterized by the acme of *Thaumatoporella parvovesiculifera* associated to *Aeolisaccus* sp.

in the upper part of Unit A, corals and large megalondontoids persist but they are characterized by thinner shells and skeleton bodies, interpreted as the beginning of the macrobenthos crises likely related to the increase of the ocean acidification (Figs. 2, 4) (Todaro et al., 2023). Successively, the base of Unit B is marked by the disappearance of the large megalodontoids and corals. After the returning to more positive values, a first prominent negative shift interpreted as I-CIE occurred at the lower part of Unit B, which testifies the decreasing diversity and size of the macrobenthic communities, as observed in the megalodontoid bivalves (Todaro et al., 2023) (Figs. 3, 4). This first I-CIE shift is recorded in a short interval, which is very rapid and distinguishable by its notable excursion value of >6‰ (Fig. 3). This C perturbation from organic matter is conspicuous compared to slightly perceptible variation documented in the $\delta^{13}C_{carb}$ in the same time interval (Todaro et al., 2017). After the first negative peak, a second significant negative-positive shift was recorded in Unit B, which is also documented in other pelagic sections (Bachan et al., 2012; Fujisaki et al., 2018; Hesselbo et al., 2002, 2004; Ruhl et al., 2009; Yager et al., 2017, 2021; Zaffani et al., 2018) (Fig. 3). We interpreted this second shift as a secondary pulse of the I-CIE, characterized by less amplitude compared to the first pulse, and occurring during a $\delta^{13}C_{org}$ returning trend to more positive values. This secondary negative shift is well visible in detailed $\delta^{13}C_{org}$ curve, where the sampling pace is thorough (Fig. 3). Afterwards, a long trend towards more negative values (from −21.7‰ to 27.2‰) starts just after the first and second shifts of the I-CIE, reaching and then persisting at values around −26.3‰ along the whole Unit C, with minor fluctuations of ±0.6‰. This long $\delta^{13}C_{org}$ decreasing trend and the successive stability at negative values represent the M-CIE, developing across the TJB (e.g. Hesselbo et al., 2002; Fujisaki et al., 2018; Zaffani et al., 2018; Du et al., 2020). The first most negative peak of M-CIE is very close to the FO of the voted primary biomarker *Psiloceras spelae* (ammonite) in Kuhjoch section (Austria) (Fig. 3), which defines the base of the Hettangian, thus the Triassic/Jurassic boundary (Hillebrandt et al., 2013). Significantly, this most negative peak at the end of the negative trend and characterizing the base of the M-CIE is consistent with the TJB biostratigraphic constrains of other pelagic sections (Fig. 3). At Mt. Sparagio, these stable and more negative values distinguishing the uppermost part of the M-CIE occur in unquestionable Jurassic rocks, as testified by the bloom of the oligotrophic *Thaumatoporella parvovesiculifera* (Fig.4), associated to problematic *Aeolisaccus* sp. and the foraminifer *Siphovalvulina* sp. (biozone LA sensu Barattolo and Romano, 2005). However, a short and significant positive peak occurred between the $\delta^{13}C_{org}$ negative trend and the stable values of organic carbon, which is very marked at Mt. Sparagio (Figs. 2, 3). This positive peak of the $\delta^{13}C_{org}$ corresponds to the acme of *T. parvovesiculifera* as firstly described by Todaro et al. (2017, 2018), marking the extinction of the Rhaetian (Triassic) macro- and micro communities (e.g. megalodontoids, *Triasina hantkeni*) (Fig. 4).

5.2. Controlling factors of the ETE at Mt Sparagio

The end Triassic Extinction (ETE) in shallow-water environments affected both reef and peritidal dwelling organisms. In reef settings, corals and hypercalcified sponges suffered the major losses of taxa (Flügel, 2002; Kiessling, 2005; Kiessling and Simpson, 2011; Stanley et al., 2013), together with the high-energy miliolid foraminifera group (e.g. *Galeanella* sp., *Siculocosta* sp., *Costifera* sp., etc.). In peritidal/lagoonal and back reef settings, the major target of the ETE consists of the bivalve megalodontoids characterized by thick aragonitic shells (McRoberts et al., 2012), along with benthic foraminifers and calcareous algae (Flügel, 2002). Besides Mt. Sparagio, at least three Tethyan peritidal sections allow to document the end-Triassic faunistic decline and the Jurassic recovery, that are the Croci d'Acerno section (De Castro, 1990), the Mt. Messapion section (Romano et al., 2008) and the section at Tataiskele (Turkey, Coskun Tunaboylu et al., 2014). All these sections record the sudden disappearance of the Rhaetian benthic community that includes bivalve megalodontoids, Triassic foraminifers and calcareous algae that are replaced by oligotrophic assemblages dominate by *Thaumatoporella parvovesiculifera*. This event is assumed as the biostratigraphic TJB in peritidal facies (biozone TA/LA sensu Barattolo and Romano, 2005). As previously reported by Todaro et al. (2017, 2018) at Mt. Sparagio, the Rhaetian subtidal beds show the presence of megalodontoids (*Megalodon* sp., *Dicerocardium* sp.) (Fig. 4), benthic foraminifera such as *Triasina hantkeni*, *Auloconus permodiscoides*, *Duotaxis birmanica*, *Tetrataxis inflata*, *Aulotortus sinuosus,* and the calcareous algae *Cayeuxia* sp., *Orthonella* sp., *Griphoporella curvata*. Along the section, this faunal association is later replaced by the oligotrophic microfacies dominated by *T. parvovesiculifera* and *Aeolisaccus* sp. that characterized the lowermost Jurassic (Fig. 4).

The main trigger of the ETE might be related to the onset of CAMP, which would have affected the dissolution (and calcification) of coral skeletons and megalodontoids as consequence of oceanic acidification (Hautmann et al., 2008). Furthermore, the decrease of calcification rates could have also been responsible of reduced growth sizes of this group of bivalves during Rhaetian (McRoberts et al., 2012), as documented also by the bivalve turnovers recorded between Unit A and B at the M. Sparagio. Greene et al. (2012) strongly supported the CAMP-induced acidification of the oceans as the most efficient triggering factor of the ETE. In addition, the development of dysoxic/anoxic conditions was reported in both deep- and shallow-water sedimentary basins, increasing the extinction rates of benthic communities (He et al., 2020, 2022; Jost et al., 2017; Luo et al., 2018). However, the individuation of the most invoked and efficient triggers among anoxia, acidification, cooling and global warming that caused the losses of many genera and species is still debated, or more probably, related to different causes working contemporaneously (Hautmann, 2004; Stanley et al., 2013).

Considering the $\delta^{13}C_{org}$ curve and the extinction trends at Mt. Sparagio it is possible to recognize different events during Rhaetian and across the TJB (Figs. 3, 4):

1) optimum of ecologic conditions favored the growth of very abundant and diversified gigantic megalodontoids associated to coral carpets and a high diverse invertebrate benthic fauna at the lower part of Unit A;
2) disappearance of the large megalodontoids and the coral carpets that are replaced by thin shelled but still large megalodontoids associated to isolated and anomalously thin branch corals in the upper part of Unit A, which was interpreted as the first signal of acidification associated to a gradual warming (Todaro et al., 2023), and corresponding to the precursor CIE;
3) drastic reduction of diversity and size of megalodontoids along Unit B, probably direct effect of the ocean acidification increasing in the lagoon environments induced by the Initial CIE;
4) abrupt extinction of all the Triassic benthic associations at the top of Unit B, corresponding to strong cooling episode, reaching cooler temperature of ca. 18–20 °C (Todaro et al., 2023) along with the spreading of dysoxic/anoxic conditions (He et al., 2020, 2022), previously described also in marginal facies of the Panormide Carbonate Platform (Scopelliti et al., 2009);
5) lasting of unfavorable ecologic conditions permitted the development of opportunistic species such as the calcareous alga *Thaumatoporella* sp.;
6) gradual reestablishment of the normal ecologic conditions allowed a gradual recovery of the benthic communities during the earliest Jurassic, recorded in the upper portion of the Main CIE.

6. Conclusions

The Mt. Sparagio section has been investigated for organic carbon isotope and we described for the first time a complete $\delta^{13}C_{org}$ profile in a Tethyan carbonate platform during the end-Triassic mass extinction event. In particular, we documented:

- the 3 negative excursions that characterized the Triassic/Jurassic boundary time interval, that are in stratigraphic order the Precursor, the Initial, and the Main CIE;
- the correspondence between the negative CIEs and the biotic turnovers documented along the Mt. Sparagio section testifies the influence of the Central Atlantic Magmatic Province also on shallow water communities across the Triassic/Jurassic boundary;
- the evidence of an extinction trend consisting of decreasing in thickness of bivalve shells and coral skeleton bodies following by the extinction of large megalodontoids and eventually of the Triassic macro and microbenthic communities characterized the ETE of carbonate platform;
- the $\delta^{13}C_{org}$ correlation between peritidal environments with pelagic successions confirms the organic carbon isotopes as a powerful tool for global correlations.

CRediT authorship contribution statement

Manuel Rigo: Writing – review & editing, Writing – original draft, Investigation, Funding acquisition, Formal analysis, Conceptualization. **Marco Favero:** Writing, Formal analysis. **Pietro di Stefano:** Writing – reviewing; Funding acquisition, Conceptualization. **Simona Todaro:** Writing – reviewing; Funding acquisition, Conceptualization.

Declaration of competing interest

The authors declare that they have no known conflict of interests or personal relationships that could have appeared to influence the work reported in this paper.

Data availability

Data will be made available on request.

Acknowledgments

This work was carried out with the financial support from the University of Padova (DOR2281100/22 and DOR2348181/23) by MR; the University of Palermo (2019_AIM_CTC_DISTEM_CI_1) by ST, (R4D14-P5F5RISS-MARGINE) by PDS.

Appendix A. Supplementary data

Supplementary data to this article can be found online at https://doi.org/10.1016/j.palaeo.2024.112440.

References

Abate, B., Di Maggio, C., Incandella, A., Renda, P., 1991. Nuovi dati sulla geologia della Penisola di Capo San Vito (Sicilia nord-occidentale). Mem. Soc. Geol. Ital. 47, 15–25.

Bachan, A., Van De Schootbrugge, B., Fiebig, J., McRoberts, C.A., Ciarapica, G., Payne, J. L., 2012. Carbon cycle dynamics following the end-Triassic mass extinction: Constraints from paired $\delta^{13}C_{carb}$ and $\delta^{13}C_{org}$ records. Geochem. Geophys. Geosyst. 13 https://doi.org/10.1029/2012GC004150, 2012GC004150.

Barattolo, F., Romano, R., 2005. Shallow carbonate platform bioevents during the Upper Triassic-Lower Jurassic; an evolutive interpretation. Boll. Soc. Geol. Ital. 124, 123–142.

Bartolini, A., Guex, J., Spangenberg, J.E., Schoene, B., Taylor, D.G., Schaltegger, U., Atudorei, V., 2012. Disentangling the Hettangian carbon isotope record: Implications for the aftermath of the end-Triassic mass extinction. Geochem. Geophys. Geosyst. 13 https://doi.org/10.1029/2011GC003807, 2011GC003807.

Coplen, T.B., Brand, W.A., Gehre, M., Gröning, M., Meijer, H.A., Toman, B., Verkouteren, R.M., 2006. New guidelines for δ 13C measurements. Anal. Chem. 78, 2439–2441.

Coskun Tunaboylu, B., Altiner, D., İsintek, İ., Demirci, D., 2014. Foraminiferal biostratigraphy and sequence stratigraphy of peritidal carbonates at the Triassic–Jurassic boundary (Karaburun Peninsula, Western Turkey). J. Asian Earth Sci. 90, 61–76. https://doi.org/10.1016/j.jseaes.2014.04.015.

Črne, A.E., Weissert, H., Goričan, Š., Bernasconi, S.M., 2011. A biocalcification crisis at the Triassic-Jurassic boundary recorded in the Budva Basin (Dinarides, Montenegro). Bulletin 123, 40–50.

Davies, J.H.F.L., Marzoli, A., Bertrand, H., Youbi, N., Ernesto, M., Schaltegger, U., 2017. End-Triassic mass extinction started by intrusive CAMP activity. Nat. Commun. 8, 15596 https://doi.org/10.1038/ncomms15596.

De Castro, P., 1990. Studies on the Triassic carbonates of the Salerno Province (Southern Italy): the Croci d'Acerno sequence. Boll. Soc. Geol. Ital. 109, 187–217.

Degen, T., Sadki, M., Bron, E., König, U., Nénert, G., 2014. The highscore suite. Powder Diffract. 29, S13–S18.

Di Stefano, P., Alessi, A., Gullo, M., 1996. Mesozoic and Paleogene megabreccias in Southern Sicily: new data on the Triassic paleomargin of the Siculo-Tunisian Platform. Facies 34, 101–122.

Du, Y., Chiari, M., Karádi, V., Nicora, A., Onoue, T., Pálfy, J., Roghi, G., Tomimatsu, Y., Rigo, M., 2020. The asynchronous disappearance of conodonts: new constraints from Triassic-Jurassic boundary sections in the Tethys and Panthalassa. Earth Sci. Rev. 203, 103176 https://doi.org/10.1016/j.earscirev.2020.103176.

Du, Y., Onoue, T., Tomimatsu, Y., Wu, Q., Rigo, M., 2023. Lower Jurassic conodonts from the Inuyama area of Japan: implications for conodont extinction. Front. Ecol. Evol. 11, 1135789.

Flügel, E., 2002. Triassic Reef Patterns.

Fujisaki, W., Matsui, Y., Asanuma, H., Sawaki, Y., Suzuki, K., Maruyama, S., 2018. Global perturbations of carbon cycle during the Triassic–Jurassic transition recorded in the mid-Panthalassa. Earth Planet. Sci. Lett. 500, 105–116.

Giunta, G., Liguori, V., 1972. Geologia dell'estremità nord-occidentale della Sicilia. Flaccovio.

Greene, S.E., Bottjer, D.J., Corsetti, F.A., Berelson, W.M., Zonneveld, J.-P., 2012. A subseafloor carbonate factory across the Triassic-Jurassic transition. Geology 40, 1043–1046. https://doi.org/10.1130/G33205.1.

Guex, J., Bartolini, A., Atudorei, V., Taylor, D., 2004. High-resolution ammonite and carbon isotope stratigraphy across the Triassic–Jurassic boundary at New York Canyon (Nevada). Earth Planet. Sci. Lett. 225, 29–41. https://doi.org/10.1016/j.epsl.2004.06.006.

Guex, J., Schoene, B., Bartolini, A., Spangenberg, J., Schaltegger, U., O'Dogherty, L., Taylor, D., Bucher, H., Atudorei, V., 2012. Geochronological constraints on post-extinction recovery of the ammonoids and carbon cycle perturbations during the Early Jurassic. Palaeogeography Palaeoclimatology Palaeoecology 346, 1–11.

Hallam, A., Wignall, P., 1999. Mass extinctions and sea-level changes. Earth Sci. Rev. 48, 217–250.

Hautmann, M., 2004. - Effect of end-Triassic CO2 maximum on carbonatesedimentation and marine mass extinction. Facies 50 (2), 257–261.

Hautmann, M., Stiller, F., Huawei, C., Jingeng, S., 2008. Extinction-recovery pattern of level-bottom faunas across the Triassic-Jurassic boundary in Tibet: implications for potential killing mechanisms. Palaios 23 (10), 711–718.

He, T., Dal Corso, J., Newton, R.J., Wignall, P.B., Mills, B.J.W., Todaro, S., Di Stefano, P., Turner, E.C., Jamieson, R.A., Randazzo, V., Rigo, M., Jones, R.E., Dunhill, A.M., 2020. An enormous sulfur isotope excursion indicates marine anoxia during the end-Triassic mass extinction. Sci. Adv. 6, eabb6704 https://doi.org/10.1126/sciadv.abb6704.

He, T., Newton, R.J., Wignall, P.B., Reid, S., Dal Corso, J., Takahashi, S., Wu, H., Todaro, S., Di Stefano, P., Randazzo, V., 2022. Shallow Ocean oxygen decline during the end-Triassic mass extinction. Glob. Planet. Chang. 210, 103770.

Hesselbo, S.P., Robinson, S.A., Surlyk, F., Piasecki, S., 2002. Terrestrial and marine extinction at the Triassic-Jurassic boundary synchronized with major carbon-cycle perturbation: a link to initiation of massive volcanism? Geol 30, 251. https://doi.org/10.1130/0091-7613(2002)030<0251:TAMEAT>2.0.CO;2.

Hesselbo, S.P., Robinson, S.A., Surlyk, F., 2004. Sea-level change and facies development across potential Triassic–Jurassic boundary horizons, SW Britain. JGS 161, 365–379. https://doi.org/10.1144/0016-764903-033.

Hillebrandt, A., Krystyn, L., Kürschner, W., Bonis, N., Ruhl, M., Richoz, S., Schobben, M., Urlichs, M., Bown, P., Kment, K., 2013. The global stratotype sections and point (GSSP) for the base of the Jurassic System at Kuhjoch (Karwendel Mountains, Northern Calcareous Alps, Tyrol, Austria). Episodes 36, 162–198.

Huynh, T.T., Poulsen, C.J., 2005. Rising atmospheric CO2 as a possible trigger for the end-Triassic mass extinction. Palaeogeogr. Palaeoclimatol. Palaeoecol. 217, 223–242. https://doi.org/10.1016/j.palaeo.2004.12.004.

Jost, A.B., Bachan, A., van De Schootbrugge, B., Lau, K.V., Weaver, K.L., Maher, K., Payne, J.L., 2017. Uranium isotope evidence for an expansion of marine anoxia during the end-T riassic extinction. Geochem. Geophys. Geosyst. 18, 3093–3108.

Kiessling, W., 2005. Long-term relationships between ecological stability and biodiversity in Phanerozoic reefs. Nature 433, 410–413.

Kiessling, W., Simpson, C., 2011. On the potential for ocean acidification to be a general cause of ancient reef crises: ANCIENT REEF CRISES. Glob. Chang. Biol. 17, 56–67. https://doi.org/10.1111/j.1365-2486.2010.02204.x.

Kiessling, W., Aberhan, M., Brenneis, B., Wagner, P.J., 2007. Extinction trajectories of benthic organisms across the Triassic–Jurassic boundary. Palaeogeogr. Palaeoclimatol. Palaeoecol. 244, 201–222. https://doi.org/10.1016/j.palaeo.2006.06.029.

Kuroda, J., Hori, R.S., Suzuki, K., Gröcke, D.R., Ohkouchi, N., 2010. Marine osmium isotope record across the Triassic-Jurassic boundary from a Pacific pelagic site. Geology 38, 1095–1098.

Laugié, M., Michel, J., Pohl, A., Poli, E., Borgomano, J., 2019. Global distribution of modern shallow-water marine carbonate factories: a spatial model based on environmental parameters. Sci. Rep. 9 (1), 1–14.

Luo, G., Richoz, S., Van De Schootbrugge, B., Algeo, T.J., Xie, S., Ono, S., Summons, R.E., 2018. Multiple sulfur-isotopic evidence for a shallowly stratified ocean following the Triassic-Jurassic boundary mass extinction. Geochim. Cosmochim. Acta 231, 73–87. https://doi.org/10.1016/j.gca.2018.04.015.

Marzoli, A., Renne, P.R., Piccirillo, E.M., Ernesto, M., Bellieni, G., Min, A.D., 1999. Extensive 200-million-year-old continental flood basalts of the Central Atlantic Magmatic Province. Science 284, 616–618.

Marzoli, A., Bertrand, H., Knight, K.B., Cirilli, S., Buratti, N., Vérati, C., Nomade, S., Renne, P.R., Youbi, N., Martini, R., Allenbach, K., Neuwerth, R., Rapaille, C., Zaninetti, L., Bellieni, G., 2004. Synchrony of the Central Atlantic magmatic province and the Triassic-Jurassic boundary climatic and biotic crisis. Geol 32, 973. https://doi.org/10.1130/G20652.1.

McElwain, J.C., Beerling, D.J., Woodward, F.I., 1999. Fossil plants and global warming at the Triassic-Jurassic boundary. Science 285, 1386–1390. https://doi.org/10.1126/science.285.5432.1386.

McRoberts, C.A., Krystyn, L., Hautmann, M., 2012. Macrofaunal response to the end-triassic mass extinction in the West-Tethyan Kossen Basin, Austria. Palaios 27, 607–616. https://doi.org/10.2110/palo.2012.p12-043r.

Nigro, F., Renda, P., 2002. From Mesozoic extension to Tertiary collision; deformation patterns in the units of the north-western Sicilian chain. Boll. Soc. Geol. Ital. 121, 87–97.

Nomade, S., Knight, K.B., Beutel, E., Renne, P.R., Verati, C., Féraud, G., Marzoli, A., Youbi, N., Bertrand, H., 2007. Chronology of the Central Atlantic Magmatic Province: implications for the Central Atlantic rifting processes and the Triassic–Jurassic biotic crisis. Palaeogeogr. Palaeoclimatol. Palaeoecol. 244, 326–344. https://doi.org/10.1016/j.palaeo.2006.06.034.

Pálfy, J., Demény, A., Haas, J., Hetényi, M., Orchard, M.J., Veto, I., 2001. Carbon isotope anomaly and other geochemical changes at the Triassic-Jurassic boundary from a marine section in Hungary. Geol 29, 1047. https://doi.org/10.1130/0091-7613(2001)029<1047:CIAAOG>2.0.CO;2.

Pálfy, J., Demény, A., Haas, J., Carter, E.S., Görög, Á., Halász, D., Oravecz-Scheffer, A., Hetényi, M., Márton, E., Orchard, M.J., Ozsvárt, P., Vető, I., Zajzon, N., 2007. Triassic–Jurassic boundary events inferred from integrated stratigraphy of the Csővár section, Hungary. Palaeogeogr. Palaeoclimatol. Palaeoecol. 244, 11–33. https://doi.org/10.1016/j.palaeo.2006.06.021.

Randazzo, V., Di Stefano, P., Todaro, S., Cacciatore, M.S., 2020. A Cretaceous carbonate escarpment from Western Sicily (Italy): biostratigraphy and tectono-sedimentary evolution. Cretac. Res. 110, 104423 https://doi.org/10.1016/j.cretres.2020.104423.

Randazzo, V., Di Stefano, P., Schlagintweit, F., Todaro, S., Cacciatore, M.S., Zarcone, G., 2021. The migration path of Gondwanian dinosaurs toward Adria: new insights from the Cretaceous of NW Sicily (Italy). Cretac. Res. 126, 104919.

Raup, D.M., Sepkoski Jr., J.J., 1984. Periodicity of extinctions in the geologic past. Proc. Natl. Acad. Sci. 81, 801–805.

Rigo, M., Onoue, T., Tanner, L.H., Lucas, S.G., Godfrey, L., Katz, M.E., Zaffani, M., Grice, K., Cesar, J., Yamashita, D., 2020. The Late Triassic Extinction at the Norian/Rhaetian boundary: biotic evidence and geochemical signature. Earth Sci. Rev. 204, 103180.

Rigo, M., Jin, X., Godfrey, L., Katz, M.E., Sato, H., Tomimatsu, Y., Zaffani, M., Maron, M., Satolli, S., Concheri, G., Cardinali, A., Wu, Q., Du, Y., Lei, J.Z.X., van Wieren, C.S., Tackett, L.S., Campbell, H., Bertinelli, A., Onoue, T., 2024. Unveiling a new Oceanic Anoxic Event at the Norian/Rhaetian Boundary (Late Triassic). Sci. Rep. 4, 15574. https://doi.org/10.1038/s41598-024-66343-z.

Romano, R., Masetti, D., Carras, N., Barattolo, F., Roghi, G., 2008. The Triassic/Jurassic boundary in a peritidal carbonate platform of the Pelagonian Domain: the Mount Messapion section (Chalkida, Greece). Riv. Ital. Paleontol. Stratigr. 114, 431–452.

Ruhl, M., Kürschner, W.M., 2011. Multiple phases of carbon cycle disturbance from large igneous province formation at the Triassic-Jurassic transition. Geology 39, 431–434. https://doi.org/10.1130/G31680.1.

Ruhl, M., Kürschner, W.M., Krystyn, L., 2009. Triassic–Jurassic organic carbon isotope stratigraphy of key sections in the western Tethys realm (Austria). Earth Planet. Sci. Lett. 281, 169–187. https://doi.org/10.1016/j.epsl.2009.02.020.

Ruhl, M., Deenen, M.H.L., Abels, H.A., Bonis, N.R., Krijgsman, W., Kürschner, W.M., 2010. Astronomical constraints on the duration of the early Jurassic Hettangian stage and recovery rates following the end-Triassic mass extinction (St Audrie's Bay/East Quantoxhead, UK). Earth Planet. Sci. Lett. 295, 262–276. https://doi.org/10.1016/j.epsl.2010.04.008.

Ruhl, M., Bonis, N.R., Reichart, G.-J., Damsté, J.S.S., Kürschner, W.M., 2011. Atmospheric carbon injection linked to end-triassic mass extinction. Science 333, 430–434. https://doi.org/10.1126/science.1204255.

Schaller, M.F., Wright, J.D., Kent, D.V., Olsen, P.E., 2012. Rapid emplacement of the Central Atlantic Magmatic Province as a net sink for CO2. Earth Planet. Sci. Lett. 323–324, 27–39. https://doi.org/10.1016/j.epsl.2011.12.028.

Scopelliti, G., Neri, R., Bellanca, A., Di Stefano, P., Barbieri, M., 2009. Sedimentology, petrography and geochemistry of a limestone breccia (*Pietra di Billiemi)* from north-West Sicily, Italy: implications for evolution of the Tethyan basins around the Triassic/Jurassic boundary. Sedimentology 56, 591–607. https://doi.org/10.1111/j.1365-3091.2008.00987.x.

Stanley, G.D., Yancey, T.E., Shepherd, H.M.E., 2013. Giant Upper Triassic bivalves of Wrangellia, Vancouver Island, Canada. Can. J. Earth Sci. 50, 142–147. https://doi.org/10.1139/cjes-2012-0025.

Thibodeau, A.M., Ritterbush, K., Yager, J.A., West, A.J., Ibarra, Y., Bottjer, D.J., Berelson, W.M., Bergquist, B.A., Corsetti, F.A., 2016. Mercury anomalies and the timing of biotic recovery following the end-Triassic mass extinction. Nat. Commun. 7, 11147. https://doi.org/10.1038/ncomms11147.

Todaro, S., Di Stefano, P., Zarcone, G., Randazzo, V., 2017. Facies stacking and extinctions across the Triassic–Jurassic boundary in a peritidal succession from western Sicily. Facies 63, 20. https://doi.org/10.1007/s10347-017-0500-5.

Todaro, S., Rigo, M., Randazzo, V., Di Stefano, P., 2018. The end-Triassic mass extinction: a new correlation between extinction events and δ13C fluctuations from a Triassic-Jurassic peritidal succession in western Sicily. Sediment. Geol. 368, 105–113. https://doi.org/10.1016/j.sedgeo.2018.03.008.

Todaro, S., Agosta, F., Parrino, N., Cavalcante, F., Di Stefano, P., Giarrusso, R., Pepe, F., Renda, P., Tondi, E., 2022a. Fracture stratigraphy and oil first migration in Triassic shales, Favignana Island, western Sicily, Italy. Mar. Pet. Geol. 135, 105400.

Todaro, S., Rigo, M., Di Stefano, P., Aiuppa, A., Chiaradia, M., 2022b. End-triassic extinction in a carbonate platform from western tethys: a comparison between extinction trends and geochemical variations. Front. Earth Sci. 10, 875466.

Todaro, S., Rigo, M., Tackett, L., Di Stefano, P., 2023. Evidence of a biodiversity crisis documented on a peritidal carbonate succession from western Tethys (Sicily): new data on the End Triassic Mass Extinction. Ital. J. Geosci. 142, 122–130.

Van De Schootbrugge, B., Payne, J.L., Tomasovych, A., Pross, J., Fiebig, J., Benbrahim, M., Föllmi, K.B., Quan, T.M., 2008. Carbon cycle perturbation and stabilization in the wake of the Triassic-Jurassic boundary mass-extinction event. Geochem. Geophys. Geosyst. 9 https://doi.org/10.1029/2007GC001914, 2007GC001914.

Ward, P.D., Haggart, J.W., Carter, E.S., Wilbur, D., Tipper, H.W., Evans, T., 2001. Sudden productivity collapse associated with the Triassic-Jurassic boundary mass extinction. Science 292, 1148–1151. https://doi.org/10.1126/science.1058574.

Ward, P.D., Garrison, G.H., Haggart, J.W., Kring, D.A., Beattie, M.J., 2004. Isotopic evidence bearing on Late Triassic extinction events, Queen Charlotte Islands, British Columbia, and implications for the duration and cause of the Triassic/Jurassic mass extinction. Earth Planet. Sci. Lett. 224, 589–600.

Ward, P.D., Garrison, G.H., Williford, K.H., Kring, D.A., Goodwin, D., Beattie, M.J., McRoberts, C.A., 2007. The organic carbon isotopic and paleontological record across the Triassic–Jurassic boundary at the candidate GSSP section at Ferguson Hill, Muller Canyon, Nevada, USA. Palaeogeogr. Palaeoclimatol. Palaeoecol. 244, 281–289. https://doi.org/10.1016/j.palaeo.2006.06.042.

Yager, J.A., West, A.J., Corsetti, F.A., Berelson, W.M., Rollins, N.E., Rosas, S., Bottjer, D. J., 2017. Duration of and decoupling between carbon isotope excursions during the end-Triassic mass extinction and Central Atlantic Magmatic Province emplacement. Earth Planet. Sci. Lett. 473, 227–236.

Yager, J.A., West, A.J., Thibodeau, A.M., Corsetti, F.A., Rigo, M., Berelson, W.M., Bottjer, D.J., Greene, S.E., Ibarra, Y., Jadoul, F., Ritterbush, K.A., Rollins, N., Rosas, S., Di Stefano, P., Sulca, D., Todaro, S., Wynn, P., Zimmermann, L., Bergquist, B.A., 2021. Mercury contents and isotope ratios from diverse depositional environments across the Triassic–Jurassic Boundary: towards a more robust mercury proxy for large igneous province magmatism. Earth Sci. Rev. 223, 103775 https://doi.org/10.1016/j.earscirev.2021.103775.

Zaffani, M., Jadoul, F., Rigo, M., 2018. A new Rhaetian $\delta^{13}C_{org}$ record: carbon cycle disturbances, volcanism, End-Triassic mass Extinction (ETE). Earth Sci. Rev. 178, 92–104.